Engineered Science
DOI: https://dx.doi.org/10.30919/es8d774

Synthesis, Structural, Magnetic, Dielectric and Optical Properties of Co Doped Cr-Zn Oxide Nanoparticles for Spintronic Devices

Supriya Balsure,[1] Vikram More,[2] Sanskruti Kadam,[3] Ramkrishna Kadam[3,*] and Ankush Kadam[1]

Abstract

Dilute magnetic semiconducting (DMS) nanoparticles of Co doped $Zn_{0.95}Cr_{0.05}O$ were synthesized by sol-gel auto-combustion technique. Crystallographic analysis was made by using X-ray diffraction (XRD) technique. Rietveld refined X-ray diffraction patterns confirm the single-phase wurtzite type crystal structure with space group p63mc. Replacement of larger Zn^{2+} ions by smaller Co^{2+} reduces the lattice parameters 'a' and 'c'. Average crystallite estimated from Scherrer equation is found to be increased from 17.6 to 22.0 nm with the addition of Co^{2+} ions. Scanning electron microscope (SEM) was used to understand the surface morphology of the samples. Average grain size obtained from SEM analysis is observed in the range of 22.1 ~ 26.5 nm. Enriched ferromagnetism is observed for Co^{2+} doped samples and the saturation magnetization increases from 0.0514 to 0.1026 emu/g. At lower frequency region both dielectric constant (ε') and dielectric loss tangent (tan δ) have higher values and decreases with increasing frequency and becomes almost constant at higher frequency region. Energy band gap (E_g) is decreases from 3.26 to 2.69 eV with the addition of Co^{2+} ions in Zn-Cr oxides. Enriched ferromagnetism and higher dielectric constant at low frequency make these materials suitable for spintronic devices.

Keywords: Rietveld refinement; Crystallite size; Saturation magnetization; Dielectric constant; Energy band gap.
Received: 17 June 2022; Revised: 20 July 2022; Accepted: 06 August 2022.
Article type: Research article.

1. Introduction

Diluted magnetic semiconducting (DMS) materials, particularly II-IV semiconductors, ME (M: Cd, Zn, Hg; E: S, Se, Te) have been subject of great interest due to their unusual properties and potential applications.[1,2] Presently, several semiconductors have been used as an efficient photocatalysts for heterogeneous photocatalysis. Relatively wide energy band gap (~3.37 eV), high excitation binding energy (~60 meV) and oxygen vacancies based moderate conducting properties make zinc oxide (ZnO) nanoparticles suitable for optoelectronic devices operating within the blue and ultraviolet (UV) region.[3] Undoped ZnO is not suitable for some photocatalytic applications due to its weak optical features and can be improved by substitution of transition metal ions or rare earth ions. Nowadays, transition metal (TM) doped ZnO nanoparticles are extensively investigated due to their wide range of applications in solar cells, light emission diodes (LED's), gas sensors, electrodes, and photocatalysts, *etc*. Also, the ZnO nanoparticles have been fabricated and used for field emission as cathode materials.[4-8] Selection of proper substitute and synthesis approach show the better control on the shape and size of crystallites which in turn design the electrical, magnetic and optical properties for desired practical applications. Substitution of TM ions such as Fe, Co, Mn, Ni and Cu can significantly tailor the electrical and semimagnetic properties of ZnO nanostructures due to their high electrical conductivity and magnetic moments.[9-12] Literature reports proved that the doping of Co^{2+} ions in ZnO significantly changed the physico-chemical properties and enhanced the anti-bacterial activities.[13-15]

Numerous synthesis approaches have been developed for

[1] *Department of Physics, Jawahar Mahavidyalaya, Anadur, Osmanabad (M.S.) India.*
[2] *Department of Physics, Rajarshi Shahu College, Pathri, Dist. Aurangabad (M.S.) India.*
[3] *Department of Physics, Shrikrishna Mahavidyalaya, Gunjoti, Osmanabad (M.S.) India.*
**Email:* ram111612@yahoo.co.in (R. Kadam)

the fabrication of ZnO nanoparticles which include both physical and chemical methods. Such synthesis methods include sol-gel auto-combustion, chemical co-precipitation, hydrothermal, solvochemical, ultra-sonication, ball milling, laser ablation, microemulsion etc. which produces homogeneous nanoparticles.[9,16-21] Among these, sol-gel synthesis approach is more reliable because it produces the homogeneous nanocrystals even at low temperature and at low cost. This method requires no expensive equipment and produces low pollutants as compared to other chemical synthesis routs.[22]

Present paper reports the structural, magnetic, optical and dielectric properties of Co doped Cr-Zn oxide nanoparticles synthesized via so-gel auto-combustion route. Co doping in Cr-Zn oxides modifies the physical properties and make them suitable for spintronic devices.

2. Materials and methods

DMS nanoparticles of Co doped Zn-Cr oxides with compositional formula $Co_xZn_{0.95-x}Cr_{0.05}O$ (x= 0.0, 0.02, 0.04, 0.06, 0.08 and 0.1) were synthesized by using sol-gel technique. Constituent elements were taken with their weight proportions in the form of AR grade metal nitrates with high purity (98.5%) in the composition. $Co(NO_3)_2.6H_2O$, $Zn(NO_3)_2.6H_2O$, $Cr(NO_3)_3.9H_2O$ and $C_6H_8O_7.H_2O$ were mixed in sufficient amount of double distilled deionized water. Table S1 (Supporting information) represents the molar concentration of the constituent elements in the composition. Citric acid was added as a chelating agent in the stoichiometric proportion of 1:3. Liquid ammonia helped to maintain the pH of the solution at 7. The whole mixture of solid solution was kept on hot plate with magnetic stirrer for continuous stirring at constant temperature of 90 °C. It took couple hours to convert the crystal clear solution into viscous sol and then the solution was suddenly converted into gel after some time. The dried gel converted in to burnt ash powders after self-ignition process with brown flints. In order to obtain the final crystals, as-prepared burnt powders were crushed and sintered at an elevated temperature of 850 °C for 6 hours. All the samples were characterized by X-ray diffraction (XRD) technique in order to understand the crystallite profile. The goniometer used to record the XRD patterns was Rigaku Ultima-IV make operated with Cu-K_α radiations (λ = 1.5406 Å) in the 2θ range of 20° to 80°. Surface morphology and grain size of the samples were estimated by using scanning electron microscope (SEM, JEOL 6390 LA). Magnetic measurements of the powder samples were performed by using vibrating sample magnetometer (Lake shore; 7404) with a maximum applied field of 15,000 Oe. Optical measurements were carried out by using UV-visible spectra on UV-2102 PCS spectrometer.

3. Results and discussion

Rietveld refinement of all the XRD patterns was performed by using FullProf software. Fig. 1 shows the refined XRD patterns of $Co_xZn_{0.95-x}Cr_{0.05}O$ (x= 0.0, 0.02, 0.04, 0.06, 0.08 and 0.1) within the 2θ range of 20° to 80°. Sharp and well indexed intensive Bragg's lines reveal the high level of crystallinity of all the samples. All the prominent reflection lines are indexed for the planes (1 0 0), (0 0 2), (1 0 1), (1 0 2), (1 1 0), (1 0 3), (2 0 0), (1 1 2), (2 0 1), (0 0 4), and (2 0 2), which correspond to the hexagonal wurtzite crystal geometry of ZnO. All the indexed lines agree well with standard crystallographic open database card No. 90-901-1663 having space group p63mc.[23] There is no any anomalous peak observed in the XRD patterns due to cobalt oxide, or other impurities, suggesting that the Co^{2+} ions are successfully incorporated in the Zn-Cr-O crystal lattice.

A close observation of XRD lines shows that the Bragg's positions are slightly shifted towards higher angles which in turn affect the lattice lengths and cell volumes.[24] Several parameters have been taken into consideration such as scale factor, overall-B factor, instrumental zero correction, full width at half maxima (FWHM) (u, v, w) parameters, positional (x, y, z) coordinators, *etc*. for Rietveld refinement of the XRD lines. Table 1 represents the structural parameters such as lattice constants (a, and c), cell volume, various R-factors (profile residual factor-R_p, weighted profile residual error-R_{wp}, expected pattern factor-R_{exp}) and goodness factor (χ^2) obtained from Rietveld refinement. Reliable values of goodness factors (Table 1) reveal the best fitting quality of the XRD patterns for Co-free and Co-doped Zn-Cr-O samples.[25] Incorporation of Co^{2+} ions in Zn-Cr oxide crystal lattice shrinkages the lattice length 'a' from 3.2487 to 3.2478 Å and 'c' from 5.2043 to 5.2035 Å.[26] This decrease is closely related to the difference in ionic radii of Co^{2+} and Zn^{2+} ions. Co^{2+} ions having smaller ionic radii (0.78 Å) replace the Zn^{2+} ions having higher ionic radii (0.83 Å), which results in shrinking of lattice lengths.[14,27] Unit cell volume for the hexagonal crystal lattice is estimated by using the relation $V = 0.866a^2c$.[28] The decreasing value of cell volume from 47.599 to 47.567 $Å^3$ is attributed to the lattice parameters 'a' and 'c'. The distortion factor 'u' is computed by putting the lattice constants in the following Equation (1):[29]

$$u = \frac{a^2}{3c^2} + 0.25 \quad (1)$$

As suggested by Bindu *et al.*,[30] the distortion factor describes the displacement of each atom with respect to the next along

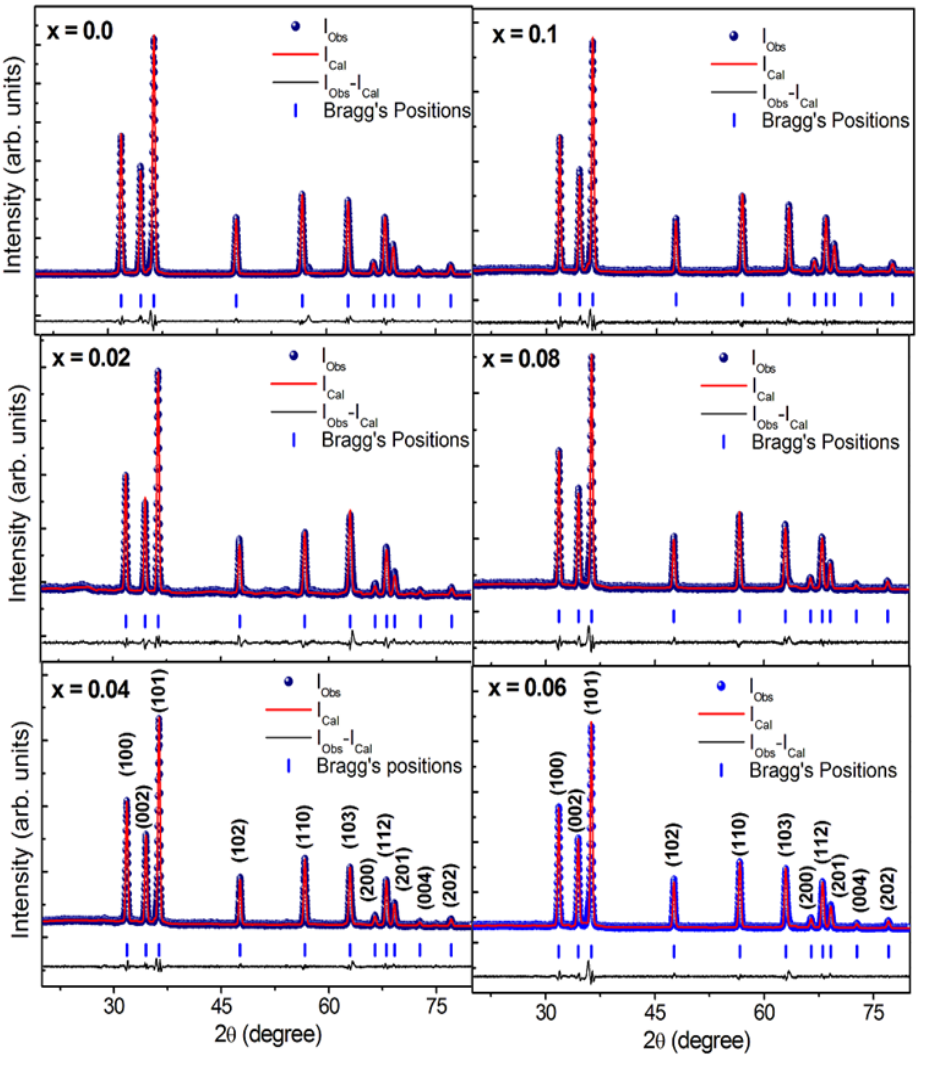

Fig. 1 Rietveld refined XRD patterns of $Co_xZn_{0.95-x}Cr_{0.05}O$ nanoparticles.

the 'c' axis.[15,30] In the present study, estimated values of distortion factor are observed very close to standard value (0.375 Å), and slightly decreased from 0.37989 to 0.37984 Å (Table 1). The fractional reduction in distortion factor is analogues with the variation in lattice parameters.

FWHM values of intensive peaks are considered for the evaluation of average crystallite size of the particles by using Debye-Scherrer Equation (2):[28]

$$t_{avg} = \frac{0.9\lambda}{\beta Cos\theta_B} \quad (2)$$

where λ - is incident X-ray wavelength (1.5406 Å), β - is full width at its half of maxima, θ_B - is the Bragg's position. It can be seen from Table 1 that the average crystallite size increases from 17.6 to 22.0 nm with the addition of Co^{2+} ions.

Field emission SEM (FE-SEM) images of typical samples x =0.02, 0.06 and 0.1 are shown in Figs. 2(a, b, and c), respectively. Average grain size was estimated by using the software Image J and the size distribution histograms are depicted in Figs. 2 (d, e, and f) for the typical samples (x = 0.02, 0.06 and 0.1) respectively. The incorporation of Co^{2+}

Table 1. Rietveld refined parameters, lattice parameters (a, c), cell volume (V) and average crystallite size (t_{avg}) of $Co_xZn_{0.95-x}Cr_{0.05}O$.

'x'	χ^2	R_P	R_{WP}	R_{Exp}	'a' (±0.002)	'c' (±0.002)	'V' (Å)^3	'u' (Å)	$t_{avg.}$ (nm)
0.0	1.71	2.51	3.15	2.41	3.2487	5.2043	47.599	0.37989	17.6
0.02	2.61	2.19	2.58	1.93	3.2486	5.2042	47.595	0.37988	19.0
0.04	3.35	2.36	2.75	1.96	3.2485	5.2041	47.591	0.37987	19.9
0.06	2.73	2.24	2.57	1.95	3.2483	5.2040	47.586	0.37986	20.4
0.08	2.81	2.27	2.63	2.05	3.2481	5.2038	47.579	0.37985	21.3
0.1	2.74	2.26	2.59	2.11	3.2478	5.2035	47.567	0.37984	22.0

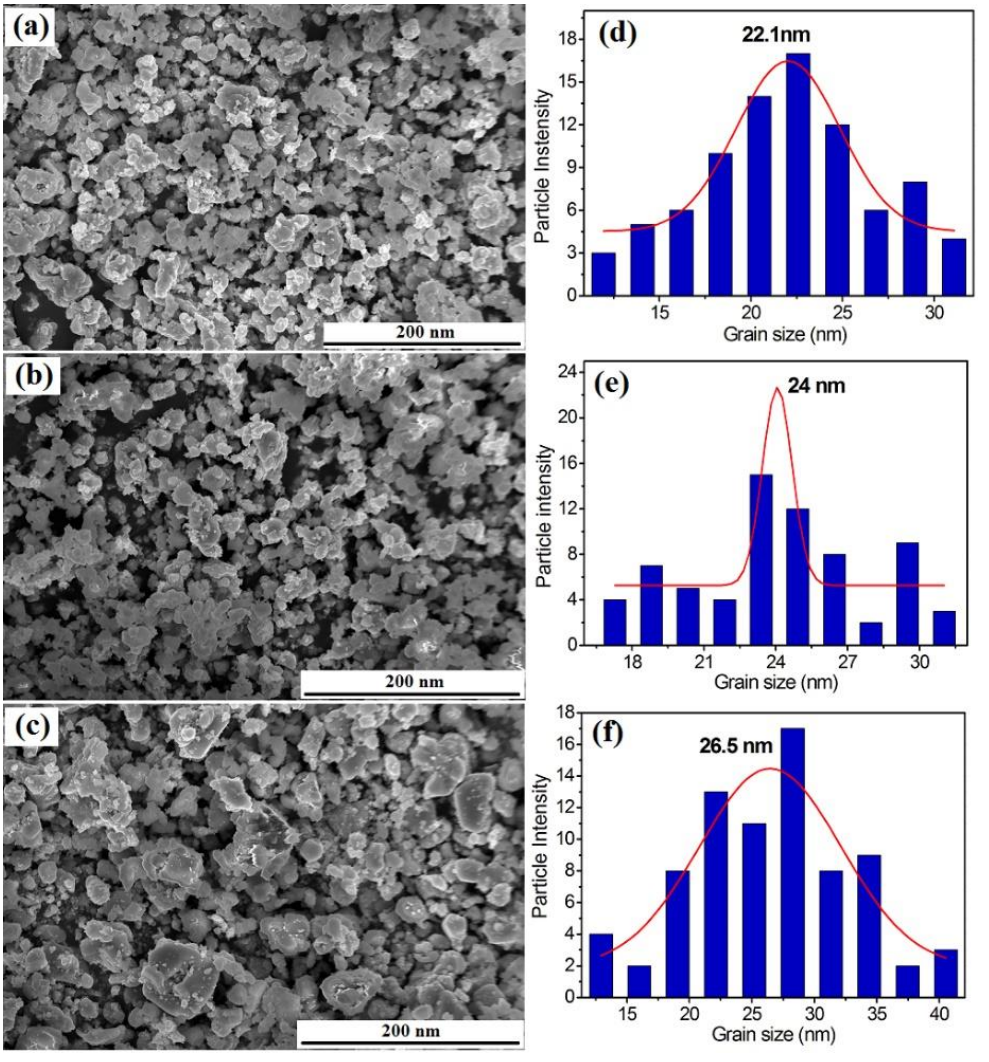

Fig. 2 FESEM images (a) x = 0.02, (b) x = 0.06 and (c) x = 0.1 and histograms (d) x = 0.02, (e) x = 0.06 and (f) x = 0.1 of $Co_xZn_{0.95-x}Cr_{0.05}O$ nanoparticles.

ions in Zn sites influences the homogeneity and morphology of the samples. As observed in SEM images, at lower doping of Co^{2+} ions (x = 0.02), distribution of nanoparticles is relatively uniform as compared to higher doping (x = 0.1). It is observed that the addition of Co^{2+} ions increases the grain size from 22.1 to 26.5 nm, which is somehow larger than the XRD results. This may be because of aggregation of primary particles which lead to the formation of secondary particles that increases grain size.[11,31]

Vibrating sample magnetometer was employed to record the M-H hysteresis loops of Co-free and Co-doped Cr-Zn oxide nanoparticles. All the measurements were carried out at room temperature by applying the magnetic field of 15 kOe. Left panel of Fig. 3 represents the M-H hysteresis loops of Co doped Cr-Zn oxides, which show the ferromagnetic behaviour of the samples at room temperature. For undoped sample, saturation magnetization (M_S) is observed 0.0514 emu/g and increases up to 0.1026 emu/g with the addition of Co^{2+} ions. The increase in M_S can be explained on the basis of high crystallinity and decreasing spin disorder on nanoparticles surface. Number of oxides like Al_2O_3, In_2O_3, CeO_2, MgO with nano-size dimension showing magnetic behaviour have the lower M_S. This magnetic behaviour is expected to originate from the exchange interactions between localized spin moments of electrons.[32-34] Right panel of Fig. 3 represents the variation of M_S and coercivity (H_C) with Co doped Zn-Cr oxides. Following Brown's relation gives the relationship between H_C and M_S:[35]

$$H_C = \frac{2K_1}{\mu_0 M_S} \quad (3)$$

In the present case, H_C of the samples decreases from 338 to 91 Oe, which is consistent with the relation shown in Equation (3). The magnetocrystalline anisotropy constant (K_1) was estimated by using the M_S and H_C values in Equation 3. Table 2 shows the values of M_S, H_C, remnant magnetization (M_r), squareness ratio (M_r/M_S) and K_1 for all the samples of

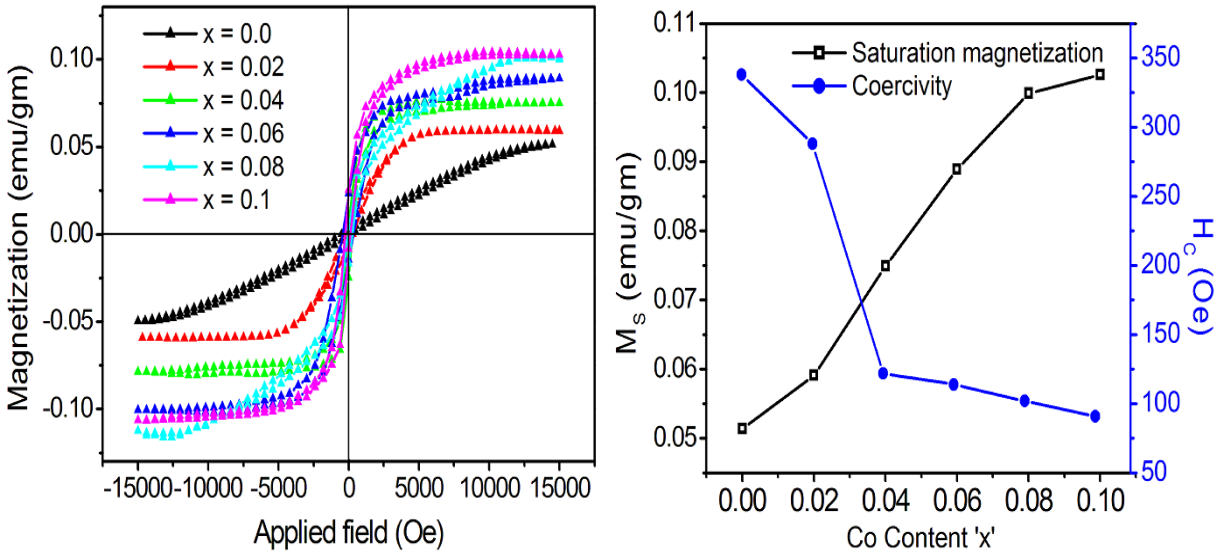

Fig. 3 (Left panel) Hysteresis loops and (Right panel) variation of saturation magnetization and coercivity for $Co_xZn_{0.95-x}Cr_{0.05}O$ nanoparticles.

$Co_xZn_{0.95-x}Cr_{0.05}O$. Values of M_r/M_S calculated for all the samples lie within the range of 0.0739 ~ 0.0591. The magnetic hardness of the materials can also be predicted by using the values of M_r/M_S.[36] It can be observed in the literature that the materials having M_r/M_S above 0.5 shows the single domain structure and lower values (<0.5) oriented from the multi-domain structures.[37] In the present case, it can be seen from Table 2, that all the samples possess multi-domain structure. The increase in saturation magnetization and decrease in H_C is desirable for application of these materials in spintronics devices.[38] Decrease in H_C restricts the magnetic and electric losses, whereas increase in M_S can generate higher spin current output.

Figure 4 shows the variation of dielectric constant (left panel) and dielectric loss tangent (right panel) as a function of frequency at room temperature for nano samples of $Co_xZn_{0.95-x}Cr_{0.05}O$. It is clear that, the values of dielectric constant

Table 2. Magnetic and optical parameters of $Co_xZn_{0.95-x}Cr_{0.05}O$

'x'	M_S (emu/g)	H_C (Oe)	M_r (emu/g)	M_r/M_S	$K_1 \times 10^{-3}$ (HA^2/kg)
0.0	0.0514	338	0.0038	0.0739	0.868
0.02	0.0591	288	0.0041	0.0694	0.851
0.04	0.0749	122	0.0046	0.0614	0.457
0.06	0.0889	114	0.0053	0.0596	0.507
0.08	0.0999	102	0.0059	0.0591	0.509
0.1	0.1026	91	0.0065	0.0634	0.467

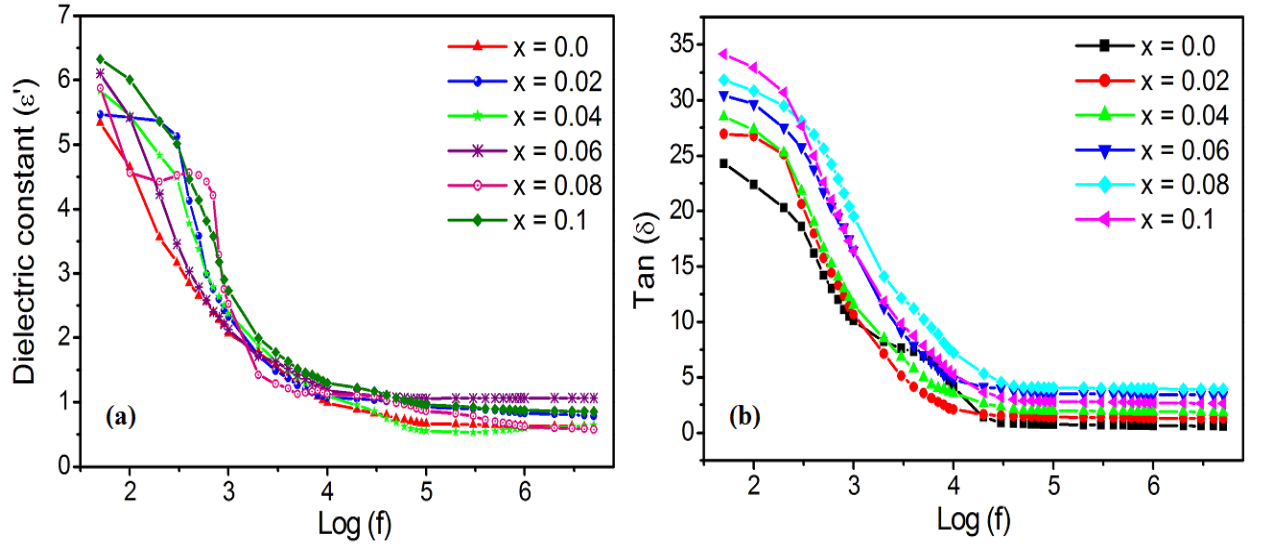

Fig. 4 Variation of (left panel) dielectric constant and (right panel) dielectric loss tangent with Log (f) for $Co_xZn_{0.95-x}Cr_{0.05}O$ nanoparticles.

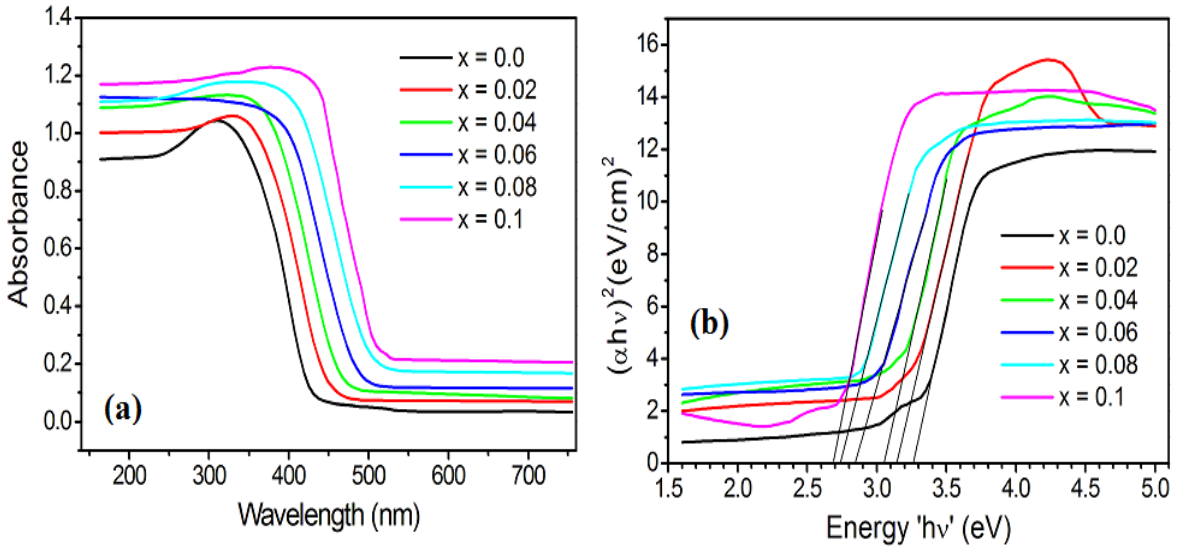

Fig. 5 Optical properties of $Co_xZn_{0.95-x}Cr_{0.05}O$ nanoparticles.

decrease with increase in the frequency. Generally, the dispersion of electron can be explained on the basis of the interfacial polarization due to the inhomogeneous dielectric structure of semiconducting materials as discussed in Koop's model, where the high observed values at low frequencies are due to the accumulation of charge carriers at the boundaries between the conductive grain regions and the highly resistive grain boundary regions.[39,40] Whereas, at high frequencies, those charges cannot follow the variation of the field and therefore their contribution to the polarization ceases. It can be easily observed that, the dielectric constant values increase for the samples substituted by Co^{2+} ions. This is because the main contributor to the dielectric constant is the interfacial polarization, which is tightly correlated to the conduction process.[41,42]

Figure 5(a) represents the UV-Vis absorption spectra of Co doped Zn-Cr oxide nanoparticles. As seen in Fig. 5(a), a strong absorption is observed below 410 nm for all the samples. Minimum absorption is observed for undoped (x = 0.0) Zn-Cr-O nanoparticles and shifted towards higher wavelengths with the addition of Co^{2+} ions and archives maxima for the sample x = 0.1. The absorption edge observed for all the samples shows considerable red shift with Co^{2+} addition, which is attributed to the agglomeration of the samples. Addition of higher magnetic ions in Zn-Cr-O lattice increases the particle agglomeration in the samples.[43,44] The increasing grain size obtained from FE-SEM analysis confirms the increasing agglomeration of the samples. For the high absorption region, the data obtained from UV-Vis absorption spectra are used to evaluate the optical band gap by employing the Tauc, David and Mott Equation (4):[11,45]

$$(\alpha h\nu)^{1/2} = A(h\nu - Eg) \quad (4)$$

where α - is absorption coefficient, ν - is frequency of light, A – is proportionality constant and E_g - is band gap energy. Fig. 5(b) shows the Tauc plots drawn between $(\alpha h\nu)^{1/2}$ and $h\nu$ for all the samples of Co doped Cr-Zn oxides. X-intercepts of extrapolated straight lines at curved portions give the values of E_g for all the samples. The addition of Co^{2+} ions decreases the E_g from 3.26 to 2.69 eV. This systematic decrease in E_g may be due to the increasing crystallite size arising from addition of Co^{2+} ions.[46] Similar results of decreasing E_g with the addition of transition metal ions in ZnO nanoparticles are observed in the previous studies.[47,48]

4. Conclusions

Co doped Zn-Cr-O wurtzite nano-crystals have been successfully fabricated by sol-gel auto combustion route. Rietveld refined parameters confirms the single phase wurtzite structure of the samples with space group p63mc. Incorporation of Co^{2+} ions in Cr-Zn-O crystal lattice reduces the lattice parameters 'a' and 'c' from 3.2487 to 3.2478 Å and 5.2043 to 5.2035 Å, respectively. Average crystallite size obtained from Scherrer equation is observed to be increased from in the range of 17.6 nm to 22.0 nm with the introduction of Co^{2+} ions. Higher doping of Co^{2+} ions increases the grain size due to aggregation of the particles. M_S is observed to be increased from 0.0514 to 0.1026 emu/g with the addition of Co^{2+} ions. Dielectric constant is found to be high at lower frequency region and decreased with increase in frequency. The decrease in E_g from 3.26 to 2.69 eV is attributed to the increase in crystallite size. The simultaneous increased ferromagnetic behavior and dielectric constant, at the same time decrease in H_C makes the Co^{2+} substituted Cr-Zn-O materials for suitable for spintronics devices.[38]

Acknowledgement
Author SDB is thankful to Punyashlok Ahilyadevi Holkar University Solapur for providing the characterization data.

Conflict of Interest
The authors declare no conflict of interest.

Supporting Information
Applicable.

References
[1] K. Rekha, M. Nirmala, M. G. Nair, A. Anukaliani, Structural, optical, photocatalytic and antibacterial activity of zinc oxide and Manganese doped zinc oxide nanoparticles, *Physica B: Condensed Matter*, 2010, **405**, 3180-3185, doi: 10.1016/j.physb.2010.04.042.
[2] J. H. Li, D. Z. Shen, J. Y. Zhang, D. X. Zhao, B. S. Li, Y. M. Lu, Y. C. Liu, X. W. Fan, The effect of Mn^{2+} doping on structure and photoluminescence of ZnO nanofilms synthesized by Sol-gel method, *Journal of Luminescence*, 2007, **122-123**, 352-354, doi: 10.1016/j.jlumin.2006.01.182.
[3] N. S. Singh, S. D. Singh, S. D. Meetei, Structural and photoluminescence properties of terbium-doped zinc oxide nanoparticles, *Chinese Physics B*, 2014, **23**, 058104, doi: 10.1088/1674-1056/23/5/058104.
[4] L. El. Mir, Luminescence properties of calcium doped zinc oxide nanoparticles, *Journal of Luminescence,* 2017, **186**, 98-102, doi: 10.1016/j.jlumin.2017.02.029.
[5] M. Krunks, A. Katerski, T. Dedova, I. Oja Acik, A. Mere, Nanostructured solar cell based on spray pyrolysis deposited ZnO nanorod array, *Solar Energy Materials and Solar Cells*, 2008, **92**, 1016-1019, doi: 10.1016/j.solmat.2008.03.002.
[6] K. Omri, L. El Mir, Effect of manganese concentration on photoluminescence properties of Zn_2SiO_4:Mn nanophosphor material, *Superlattices and Microstructures,* 2014, **70**, 24-32, doi: 10.1016/j.spmi.2014.02.022.
[7] M. C. Carotta, A. Cervi, V. di Natale, S. Gherardi, A. Giberti, V. Guidi, D. Puzzovio, B. Vendemiati, G. Martinelli, M. Sacerdoti, D. Calestani, A. Zappettini, M. Zha, L. Zanotti, ZnO gas sensors: a comparison between nanoparticles and nanotetrapods-based thick films, *Sensors and Actuators B: Chemical*, 2009, **137**, 164-169, doi: 10.1016/j.snb.2008.11.007.
[8] X.-P. Wang, Z. Wang, L.-J. Wang, C.-Y. Mei, Synthesis of ZnO films with a special texture and enhanced field emission properties, *Chinese Physics B*, 2011, **20**, 105203, doi: 10.1088/1674-1056/20/10/105203.
[9] T. C. Bharat, Shubham, S. Mondal, H. S. Gupta, P. K. Singh, A. K. Das, Synthesis of doped zinc oxide nanoparticles: a review, *Materials Today: Proceedings*, 2019, **11**, 767-775, doi: 10.1016/j.matpr.2019.03.041.
[10] S. Kumaresan, K. Vallalperuman, S. Sathishkumar, M. Karthik, P. SivaKarthik, Synthesis and systematic investigations of Al and Cu-doped ZnO nanoparticles and its structural, optical and photo-catalytic properties, *Journal of Materials Science: Materials in Electronics*, 2017, **28**, 9199-9205, doi: 10.1007/s10854-017-6654-7.
[11] M. Sajjad, I. Ullah, M. I. Khan, J. Khan, M. Y. Khan, M. T. Qureshi, Structural and optical properties of pure and copper doped zinc oxide nanoparticles, *Results in Physics*, 2018, **9**, 1301-1309, doi: 10.1016/j.rinp.2018.04.010.
[12] B. Allabergenov, S.-H. Chung, S. M. Jeong, S. Kim, B. Choi, Enhanced blue photoluminescence realized by copper diffusion doping of ZnO thin films, *Optical Materials Express*, 2013, **3**, 1733, doi: 10.1364/ome.3.001733.
[13] D. Bresser, F. Mueller, M. Fiedler, S. Krueger, R. Kloepsch, D. Baither, M. Winter, E. Paillard, S. Passerini, Transition-metal-doped zinc oxide nanoparticles as a new lithium-ion anode material, *Chemistry of Materials*, 2013, **25**, 4977-4985, doi: 10.1021/cm403443t.
[14] Y. Kumar, A. Sahai, S. F. Olive-Méndez, N. Goswami, V. Agarwal, Morphological transformations in cobalt doped zinc oxide nanostructures: effect of doping concentration, *Ceramics International*, 2016, **42**, 5184-5194, doi: 10.1016/j.ceramint.2015.12.041.
[15] P. Shunmuga Sundaram, T. Sangeetha, S. Rajakarthihan, R. Vijayalaksmi, A. Elangovan, G. Arivazhagan, XRD structural studies on cobalt doped zinc oxide nanoparticles synthesized by coprecipitation method: Williamson-Hall and size-strain plot approaches, *Physica B: Condensed Matter*, 2020, **595**, 412342, doi: 10.1016/j.physb.2020.412342.
[16] S. Cimitan, S. Albonetti, L. Forni, F. Peri, D. Lazzari, Solvothermal synthesis and properties control of doped ZnO nanoparticles, *Journal of Colloid and Interface Science*, 2009, **329**, 73-80, doi: 10.1016/j.jcis.2008.09.060.
[17] V. More, R. B. Borade, K. Desai, V. K. Barote, S. S. Kadam, V. S. Shinde, D. R. Kulkarni, R. H. Kadam, S. T. Alone, Site occupancy, surface morphology and mechanical properties of Ce^{3+} added Ni-Mn-Zn ferrite nanocrystals synthesized via Sol-gel route, *Nano*, 2021, **16**, 2150059, doi: 10.1142/s1793292021500594.
[18] G. Kasi, K. Viswanathan, K. Sadeghi, J. Seo, Optical, thermal, and structural properties of polyurethane in Mg-doped zinc oxide nanoparticles for antibacterial activity, *Progress in Organic Coatings*, 2019, **133**, 309-315, doi: 10.1016/j.porgcoat.2019.04.066.
[19] T. Dippong, I. G. Deac, O. Cadar, E. A. Levei, I. Petean, Impact of Cu^{2+} substitution by Co^{2+} on the structural and magnetic properties of $CuFe_2O_4$ synthesized by Sol-gel route, *Materials Characterization*, 2020, **163**, 110248, doi: 10.1016/j.matchar.2020.110248.
[20] T. Dippong, E. A. Levei, F. Goga, I. Petean, A. Avram, O. Cadar, The impact of polyol structure on the formation of $Zn_{0.6}Co_{0.4}Fe_2O_4$ spinel-based pigments, *Journal of Sol-Gel Science and Technology*, 2019, **92**, 736-744, doi: 10.1007/s10971-019-05140-x.
[21] T. Dippong, E.-A. Levei, C. L. Lengauer, A. Daniel, D. Toloman, O. Cadar, Investigation of thermal, structural, morphological and photocatalytic properties of $Cu_xCo_{1-x}Fe_2O_4$ ($0 \leq x \leq 1$) nanoparticles embedded in SiO_2 matrix, *Materials*

Characterization, 2020, **163**, 110268, doi: 10.1016/j.matchar.2020.110268.
[22] S. S. Satpute, S. R. Wadgane, K. Desai, D. R. Mane, R. H. Kadam, Substitution effect of Y^{3+} ions on the structural, magnetic and electrical properties of cobalt ferrite nanoparticles, *Cerâmica*, 2020, **66**, 43-49, doi: 10.1590/0366-69132020663772734.
[23] Y.-N. Xu, W. Y. Ching, Electronic, optical, and structural properties of some wurtzite crystals, *Physical Review B*, 1993, **48**, 4335-4351, doi: 10.1103/physrevb.48.4335.
[24] K. R. Desai, S. T. Alone, S. R. Wadgane, S. E. Shirsath, K. M. Batoo, A. Imran, E. H. Raslan, M. Hadi, M. F. Ijaz, R. H. Kadam, X-ray diffraction-based Williamson-Hall analysis and rietveld refinement for strain mechanism in Mg-Mn co-substituted $CdFe_2O_4$ nanoparticles, *Physica B: Condensed Matter*, 2021, **614**, 413054, doi: 10.1016/j.physb.2021.413054.
[25] Z. Feng, Q. Hou, Y. Zheng, W. Ren, J.-Y. Ge, T. Li, C. Cheng, W. Lu, S. Cao, J. Zhang, T. Zhang, Method of artificial intelligence algorithm to improve the automation level of Rietveld refinement, *Computational Materials Science*, 2019, **156**, 310-314, doi: 10.1016/j.commatsci.2018.10.006.
[26] S. Balsure, V. More, S. Kadam, D. Kulkarni, Y. Vijapure, A. Kadam, Complete X-ray Peak Profile Analysis of CoxZn0.95-xCr0.05O nanoparticles based on Williamson–Hall and SSP Methods, *International Journal of Innovative Research in Science, Engineering and Technology,* 2021, **10**, 6907-6913, doi: 10.15680/IJIRSET.2021.1006168.
[27] S. K. Gurav, S. E. Shirsath, R. H. Kadam, D. R. Mane, Low temperature synthesis of $Li_{0.5}Zr_xCo_xFe_{2.5-2x}O_4$ powder and their characterizations, *Powder Technology*, 2013, **235**, 485-492, doi: 10.1016/j.powtec.2012.11.009.
[28] S. S. Satpute, S. R. Wadgane, S. R. Kadam, D. R. Mane, R. H. Kadam, Y^{3+} substituted Sr-hexaferrites: Sol-gel synthesis, structural, magnetic and electrical characterization, *Cerâmica*, 2019, **65**, 274-281, doi: 10.1590/0366-69132019653742582.
[29] U. Godavarti, V. D. Mote, M. Dasari, Role of cobalt doping on the electrical conductivity of ZnO nanoparticles, *Journal of Asian Ceramic Societies*, 2017, **5**, 391-396, doi: 10.1016/j.jascer.2017.08.002.
[30] P. Bindu, S. Thomas, Estimation of lattice strain in ZnO nanoparticles: X-ray peak profile analysis, *Journal of Theoretical and Applied Physics*, 2014, **8**, 123-134, doi: 10.1007/s40094-014-0141-9.
[31] N. Goswami, A. Sahai, Structural transformation in nickel doped zinc oxide nanostructures, *Materials Research Bulletin*, 2013, **48**, 346-351, doi: 10.1016/j.materresbull.2012. 10.045.
[32] T. Dippong, O. Cadar, I. G. Deac, M. Lazar, G. Borodi, E. A. Levei, Influence of ferrite to silica ratio and thermal treatment on porosity, surface, microstructure and magnetic properties of $Zn_{0.5}Ni_{0.5}Fe_2O_4/SiO_2$ nanocomposites, *Journal of Alloys and Compounds*, 2020, **828**, 154409, doi: 10.1016/j.jallcom.2020.154409.
[33] T. Dippong, E.-A. Levei, I. G. Deac, F. Goga, O. Cadar, Investigation of structural and magnetic properties of NixZn1-xFe2O4/SiO2 (0≤x≤1) spinel-based nanocomposites, *Journal of Analytical and Applied Pyrolysis*, 2019, **144**, 104713, doi: 10.1016/j.jaap.2019.104713.
[34] T. Dippong, E. A. Levei, I. G. Deac, E. Neag, O. Cadar, Influence of Cu^{2+}, Ni^{2+}, and Zn^{2+} ions doping on the structure, morphology, and magnetic properties of Co-ferrite embedded in SiO_2 matrix obtained by an innovative Sol-gel route, *Nanomaterials*, 2020, **10**, 580, doi: 10.3390/nano10030580.
[35] A. A. Birajdar, S. E. Shirsath, R. H. Kadam, M. L. Mane, D. R. Mane, A. R. Shitre, Permeability and magnetic properties of Al^{3+} substituted $Ni_{0.7}Zn_{0.3}Fe_2O_4$ nanoparticles, *Journal of Applied Physics*, 2012, **112**, 053908, doi: 10.1063/1.4748959.
[36] C. C. Chauhan, A. R. Kagdi, R. B. Jotania, A. Upadhyay, C. S. Sandhu, S. E. Shirsath, S. S. Meena, Structural, magnetic and dielectric properties of Co-Zr substituted M-type calcium hexagonal ferrite nanoparticles in the presence of α-Fe_2O_3 phase, *Ceramics International*, 2018, **44**, 17812-17823, doi: 10.1016/j.ceramint.2018.06.249.
[37] A. R. Kagdi, N. P. Solanki, F. E. Carvalho, S. S. Meena, P. Bhatt, R. C. Pullar, R. B. Jotania, Influence of Mg substitution on structural, magnetic and dielectric properties of X-type Barium zinc hexaferrites $Ba_2Zn_{2-x}Mg_xFe_{28}O_{46}$, *Journal of Alloys and Compounds*, 2018, **741**, 377-391, doi: 10.1016/j.jallcom.2018.01.092.
[38] A. Hirohata, K. Yamada, Y. Nakatani, I.-L. Prejbeanu, B. Diény, P. Pirro, B. Hillebrands, Review on spintronics: principles and device applications, *Journal of Magnetism and Magnetic Materials*, 2020, **509**, 166711, doi: 10.1016/j.jmmm.2020.166711.
[39] T. Abdel-Baset, S. Saber, S. El-Sayed, Dielectric relaxations and optical properties of Mn-doped ZnO nanoparticles, *Journal of Materials Science: Materials in Electronics*, 2020, **31**, 20972-20983, doi: 10.1007/s10854-020-04611-0.
[40] I. Ben Elkamel, N. Hamdaoui, A. Mezni, R. Ajjel, Enhancement of dielectric properties of Ni and Co doped ZnO due to the oxygen vacancies for UV photosensors application, *Physica E: Low-Dimensional Systems and Nanostructures*, 2020, **119**, 114031, doi: 10.1016/j.physe.2020.114031.
[41] S. S. Choudhari, S. B. Shelke, K. M. Batoo, S. F. Adil, A. B. Kadam, A. Imran, M. Hadi, E. H. Raslan, S. E. Shirsath, R. H. Kadam, $Mn_{0.7}Zn_{0.3}Fe_2O^{4+}$ $BaTiO_3$ composites: structural, morphological, magnetic, M-E effect and dielectric properties, *Journal of Materials Science: Materials in Electronics*, 2021, **32**, 10308-10319, doi: 10.1007/s10854-021-05686-z.
[42] R. H. Kadam, R. B. Borade, M. L. Mane, D. R. Mane, K. M. Batoo, S. E. Shirsath, Structural, mechanical, dielectric properties and magnetic interactions in Dy^{3+}-substituted Co-Cu-Zn nanoferrites, *RSC Advances*, 2020, **10**, 27911-27922, doi: 10.1039/d0ra05274d.
[43] S. S. Kumar, P. Venkateswarlu, V. R. Rao, G. N. Rao, Synthesis, characterization and optical properties of zinc oxide nanoparticles, *International Nano Letters*, 2013, **3**, 30, doi: 10.1186/2228-5326-3-30.
[44] B. Baruwati, D. K. Kumar, S. V. Manorama, Hydrothermal synthesis of highly crystalline ZnO nanoparticles: a competitive sensor for LPG and EtOH, *Sensors and Actuators B: Chemical*, 2006, **119**, 676-682, doi: 10.1016/j.snb.2006.01.028.

[45] R. Krithiga, G. Chandrasekaran, Synthesis, strucutral and optical properties of vanadium doped zinc oxide nanograins, *Journal of Crystal Growth*, 2009, **311**, 4610-4614, doi: 10.1016/j.jcrysgro.2009.08.033.
[46] R. Elilarassi, G. Chandrasekaran, Synthesis and optical properties of Ni-doped zinc oxide nanoparticles for optoelectronic applications, *Optoelectronics Letters*, 2010, **6**, 6-10, doi: 10.1007/s11801-010-9236-y.
[47] S. Muthukumaran, R. Gopalakrishnan, Structural, FTIR and photoluminescence studies of Cu doped ZnO nanopowders by co-precipitation method, *Optical Materials*, 2012, **34**, 1946-1953, doi: 10.1016/j.optmat.2012.06.004.
[48] M. Ferhat, A. Zaoui, R. Ahuja, Magnetism and band gap narrowing in Cu-doped ZnO, *Applied Physics Letters*, 2009, **94**, 142502, doi: 10.1063/1.3112603.

Author Information

Supriya Balsure *pursued her Ph.D. degree (2022) from Dr. Babasaheb Ambedkar Marathwada University, Aurangabad in the field of materials science. Her research area is in the field of metal oxides specially the zinc oxide. She has published 18 research papers in various journals.*

Vikram More *has completed his Ph.D. degree in the year 2022 from Dr. B. A. M. University Aurangabad. Presently he is working at Sant Dnyaneshwar Mahavidyalaya, Soyegaon. He has published 05 research papers in reputed journals. His area of interest is in Materials Science, in particular magnetic oxide nanoparticles.*

Sanskruti Kadam *is perusing her Ph.D. degree from Dr. Babasaheb Ambedkar Marathwada University, Aurangabad in the field of materials science. Her research area is in the field of spinel ferrites with rare earth doping. She has published 05 research papers in various journals.*

Ramkrishna Kadam *is presently working as Professor in Physics at Shrikrishna Mahavidyalaya, Gunjoti, Tq. Omerga, Dist. Osmanabad (M.S.) India. He is research supervisor and his area of research is in the field of Materials Science. He has published 90 research papers and granted one Australian patent in the year 2021.*

Ankush Kadam *is presently working as Professor in Physics at Jawahar College. Anadur, Dist. Osmanabad (M.S.) India. He is research supervisor and his area of research is spinel ferrites. He has published 49 research papers in various journals.*

Publisher's Note: Engineered Science Publisher remains neutral with regard to jurisdictional claims in published maps and institutional affiliations.